Earth and Planetary Science Letters 415 (2015) 142–153

Contents lists available at ScienceDirect

Earth and Planetary Science Letters

www.elsevier.com/locate/epsl

Lower Cretaceous Xigaze ophiolites formed in the Gangdese forearc: Evidence from paleomagnetism, sediment provenance, and stratigraphy

Wentao Huang [a,b,*], Douwe J.J. van Hinsbergen [b], Marco Maffione [b], Devon A. Orme [c], Guillaume Dupont-Nivet [a,b,d,e], Carl Guilmette [f], Lin Ding [g], Zhaojie Guo [a], Paul Kapp [c]

[a] Key Laboratory of Orogenic Belts and Crustal Evolution, Ministry of Education, School of Earth and Space Sciences, Peking University, Beijing 100871, China
[b] Department of Earth Sciences, Utrecht University, Budapestlaan 17, 3584 CD, Utrecht, The Netherlands
[c] Department of Geosciences, University of Arizona, Tucson, AZ 85721, USA
[d] Géosciences Rennes, UMR 6118, Université de Rennes 1, Campus de Beaulieu, 35042 Rennes Cedex, France
[e] Institute of Earth and Environmental Science, University of Potsdam, Karl-Liebknecht-Str. 24-25, 14476 Potsdam-Golm, Germany
[f] Département de Géologie et de Génie Géologique, Université Laval, Québec, QC, Canada G1K 7P4
[g] Key Laboratory of Continental Collision and Plateau Uplift, Institute of Tibetan Plateau Research, Chinese Academy of Sciences, Beijing, China

ARTICLE INFO

Article history:
Received 12 November 2014
Received in revised form 13 January 2015
Accepted 18 January 2015
Available online 14 February 2015
Editor: A. Yin

Keywords:
Xigaze ophiolite
sedimentary contact
paleomagnetism and rock magnetism
inclination shallowing

ABSTRACT

The India–Asia suture zone of southern Tibet exposes Lower Cretaceous Xigaze ophiolites and radiolarian cherts, and time-equivalent Asian-derived clastic forearc sedimentary rocks (Xigaze Group). These ophiolites have been interpreted to have formed in the forearc of the north-dipping subduction zone below Tibet that produced the Gangdese magmatic arc around 15–20°N, or in the forearc of a sub-equatorial intra-oceanic subduction zone. To better constrain the latitude of the ophiolites, we carried out an integrated paleomagnetic, geochronologic and stratigraphical study on epi-ophiolitic radiolarites (Chongdui and Bainang sections), and Xigaze Group turbiditic sandstones unconformably overlying the ophiolite's mantle units (Sangsang section). Detrital zircon U–Pb geochronology of tuffaceous layers from the Chongdui section and sandstones of the Xigaze Group at the Sangsang section provides maximum depositional ages of 116.5 ± 3.1 Ma and 128.8 ± 3.4 Ma, respectively, for the Chongdui section and an Asian provenance signature for the Xigaze Group. Paleomagnetic analyses, integrated with rock magnetic experiments, indicate significant compaction-related inclination 'shallowing' of the remanence within the studied rocks. Two independent methods are applied for the inclination shallowing correction of the paleomagnetic directions from the Sangsang section, yielding consistent mean paleolatitudes of 16.2°N [13°N, 20.9°N] and 16.8°N [11.1°N, 23.3°N], respectively. These results are indistinguishable from recent paleolatitude estimates for the Gangdese arc in southern Tibet. Radiolarites from the Chongdui and Bainang sections yield low paleomagnetic inclinations that would suggest a sub-equatorial paleolatitude, but the distribution of the paleomagnetic directions in these rocks strongly suggests a low inclination bias by compaction. Our data indicate that spreading of the Xigaze ophiolite occurred in the Gangdese forearc, and formed the basement of the forearc strata.

1. Introduction

The Yarlung Zangbo suture zone, which separates the Lhasa terrane of Asia to the north from the India-derived Himalayan fold-thrust belt to the south, contains remnants of Neotethyan oceanic lithosphere (ophiolites) (Hébert et al., 2012) and a thick sequence of clastic sedimentary rocks derived from the Lhasa terrane forming the Xigaze Group (e.g., Wu et al., 2010; An et al., 2014; Orme et al., 2014). The oceanic crust of the ophiolites of southern Tibet formed in the Early Cretaceous above a subduction zone that accommodated India–Asia convergence, and the closure of the Neotethys Ocean (e.g., Searle et al., 1987; Yin and Harrison, 2000). Geochemical constraints suggest that these ophiolites formed in an upper plate above a subduction zone (Hébert et al., 2012). Following a long-lived subduction history, these ophiolites em-

* Corresponding author at: Department of Earth Sciences, Utrecht University, Budapestlaan 17, 3584 CD, Utrecht, The Netherlands. Tel.: +31 62 671 8388.
E-mail address: W.Huang@uu.nl (W. Huang).

http://dx.doi.org/10.1016/j.epsl.2015.01.032
0012-821X/

placed onto the northernmost continental margin strata of the Indian plate (i.e. the Tibetan Himalaya) (e.g., Ding et al., 2005; Guilmette et al., 2009; Hu et al., 2014).

The Xigaze ophiolite belt, exposed between Dazhuqu to the east and Sangsang to the west (Fig. 1), represents the largest, most complete, and best-studied Yarlung Zangbo ophiolites of southern Tibet. Contrasting views exist, however, on the location of the subduction zone above which these ophiolites formed, and on the timing of their emplacement onto the Tibetan Himalaya. Searle et al. (1987) and Corfield et al. (2001) argue for a ∼70 Ma emplacement age for the Spontang ophiolite, assuming that mafic debris in the Tibetan Himalayan strata of this age was ophiolite-derived. Paleomagnetic constraints show that the Tibetan Himalaya arrived at equatorial latitudes shortly after 70 Ma (Patzelt et al., 1996; Dupont-Nivet et al., 2010b) and such an old emplacement age would thus be consistent with an equatorial paleolatitude of this inferred intra-oceanic subduction zone (e.g., Aitchison et al., 2007). In contrast, Garzanti and Hu (2014) showed that chromium spinels in the mafic debris had a geochemical signature that is not consistent with a derivation from ophiolitic rocks, but from an (an-orogenic) mantle plume source instead. Base on the first arrival of chromium spinels with a composition consistent with the ophiolites in the Tibetan Himalaya strata, an early Eocene first erosion age of the ophiolites was suggested instead (Garzanti and Hu, 2014; Hu et al., 2014), consistent with the late Paleocene – early Eocene collision age of the Tibetan Himalaya with Tibet (e.g., Dupont-Nivet et al., 2010a; Najman et al., 2010; DeCelles et al., 2014; Lippert et al., 2014; Orme et al., 2014). This would rather suggest that the Xigaze ophiolite represents the basement of the forearc of the long-lived Gangdese arc that formed on Lhasa terrane due to subduction below the southern Tibetan margin (e.g., He et al., 2007; Lee et al., 2009).

Another factor that has contributed to the debate about the origin of the Xigaze ophiolite is that its contact with Xigaze forearc strata is in many/most places a strand of the north-directed Miocene Great Counter thrust system (e.g., Yin et al., 1999). Aitchison et al. (2003) argued that the contact was everywhere a thrust along which thousands of kilometers of convergence may have been accommodated between the ophiolites and Xigaze forearc strata. Other authors, however, reported an unconformable, or interfingering depositional relationship between the forearc strata and ophiolitic basement rocks or its radiolarian cover, respectively (e.g., Pozzi et al., 1984; An et al., 2014). Assessing the structural relationship between the forearc strata and the ophiolites, and determining the paleolatitude of the ophiolite's cover sediments (radiolarites) and the basal forearc sequence can thus provide a primary control on the subduction configuration of the Neotethys during India–Asia convergence.

So far, paleomagnetically constrained estimates of the paleolatitude of the ophiolites provided contrasting results. Pozzi et al. (1984) estimated a paleolatitude of 10–20°N for radiolarian cherts and limestones and thus suggested a near-Lhasa origin, whereas Abrajevitch et al. (2005) reported results from radiolarites, mudrocks and volcaniclastic rocks, indicating a near-equatorial paleolatitude and therefore suggested that the ophiolites formed above an intra-oceanic subduction zone unrelated to the Gangdese arc. Both datasets are small, however, and do not allow assessment of potential paleomagnetic and rock magnetic artifacts such as inclination shallowing due to sediment compaction.

In this paper, we investigate three lower Cretaceous sedimentary sections overlying the Xigaze ophiolite belt. Their field relationships with the ophiolites are described in detail. The age and provenance of the lower Cretaceous units were determined by using U–Pb zircon geochronology. Paleolatitudinal estimates were obtained from paleomagnetic analyses integrated with rock magnetic experiments, and magnetic fabric analyses, including anisotropy of magnetic susceptibility (AMS) and anisotropy of anhysteretic remanent magnetization (AARM). We specifically test for shallowing of the paramagnetic inclination, calculate a corrected paleolatitude and discuss the implications for plate reconstructions of the Neotethys.

2. Geological background and sampling

The studied Xigaze ophiolite is part of the ophiolite belt that stretches for ∼2000 km along the Yarlung Zangbo suture zone (Fig. 1a). These ophiolites structurally overlie an ophiolitic mélange to the south, and are variably structurally or depositionally overlain by sedimentary rocks of the Xigaze Group to the north (Figs. 1b, c). The Xigaze ophiolite belt is discontinuous, with the most complete sections composed of serpentinized mantle peridotites, minor cumulates, gabbros, sheeted sills and dikes, pillow basalts, and radiolarian cherts. In most places, the ophiolite succession is incomplete, and the crustal section is thin or absent. Where ophiolitic bodies are absent, the Xigaze Group is juxtaposed against ophiolitic mélange to the south (Figs. 1b, c). Based on zircon U–Pb and hornblende $^{40}Ar/^{39}Ar$ dating, the reported age of the magmatic ophiolite crust is 123–128 Ma (e.g., Guilmette et al., 2009; Dai et al., 2013). This is consistent with a Barremian to Albian age inferred from radiolarian biostratigraphy of the ophiolite's cover sediments (Aitchison et al., 2003; Ziabrev et al., 2003).

The base of the Xigaze Group comprises a marine, turbidite-dominated clastic sequence with detritus derived from Jurassic-Eocene igneous rocks of the Gangdese magmatic arc in southern Tibet (e.g., Lee et al., 2009). It was deposited in a system of forearc basins located between the arc and the associated trench (An et al., 2014; Orme et al., 2014).

We studied the ophiolite's sedimentary cover at three main localities: Chongdui, Bainang, and Sangsang (Fig. 1). The Chongdui section, near the village of Chongdui (GPS: 29.14575°N, 89.01295°E; Fig. 1b) consists of south-dipping overturned red-greenish cherts intercalating with deep-marine sandy turbidites interbedded with tuffceous sandstone layers (Figs. 2a–c). A late Barremian–late Aptian age for the cherts was reported by Ziabrev et al. (2003) based on radiolarian biostratigraphy. We collected 45 orientated hand samples (smooth planar bedding surfaces of the blocks were oriented with a magnetic compass) from the red chert layers in the field that were subsequently drilled to obtain standard paleomagnetic cores. Two hand samples (CH-UP-1 and CH-UP-3) were also collected from the tuffceous layer for U–Pb geochronologic analyses.

A total of 50 oriented hand samples were collected from the Bainang section (GPS: 29.15808°N, 89.26775°E; Figs. 1b, 2d–f) exposing Aptian greenish cherts interbedded with dark-gray turbiditic sandstones and mudstones, unconformably overlying (or interfingering with) pillow basalts. A total of 139 paleomagnetic cores were drilled at the Sangsang section (GPS: 29.34388°N, 86.61663°E; Fig. 1c) and orientated with magnetic and sun compasses. Here, mildly deformed, steeply dipping sequence of deep-marine brown-grew turbiditic sandstones interbedded with greenish thin-bedded mudstones unconformably overlies strongly deformed serpentinized peridotites (Figs. 2g–i). We collected sample SSH01132 from the base of this sequence immediately above the unconformity to determine a maximum depositional age from detrital zircon U–Pb geochronology, and to test whether the zircon age spectrum of these rocks is indicative of a Lhasa provenance.

3. Geochronology

The three samples collected for geochronology were prepared and analyzed using protocols at the Arizona Laserchron Center and

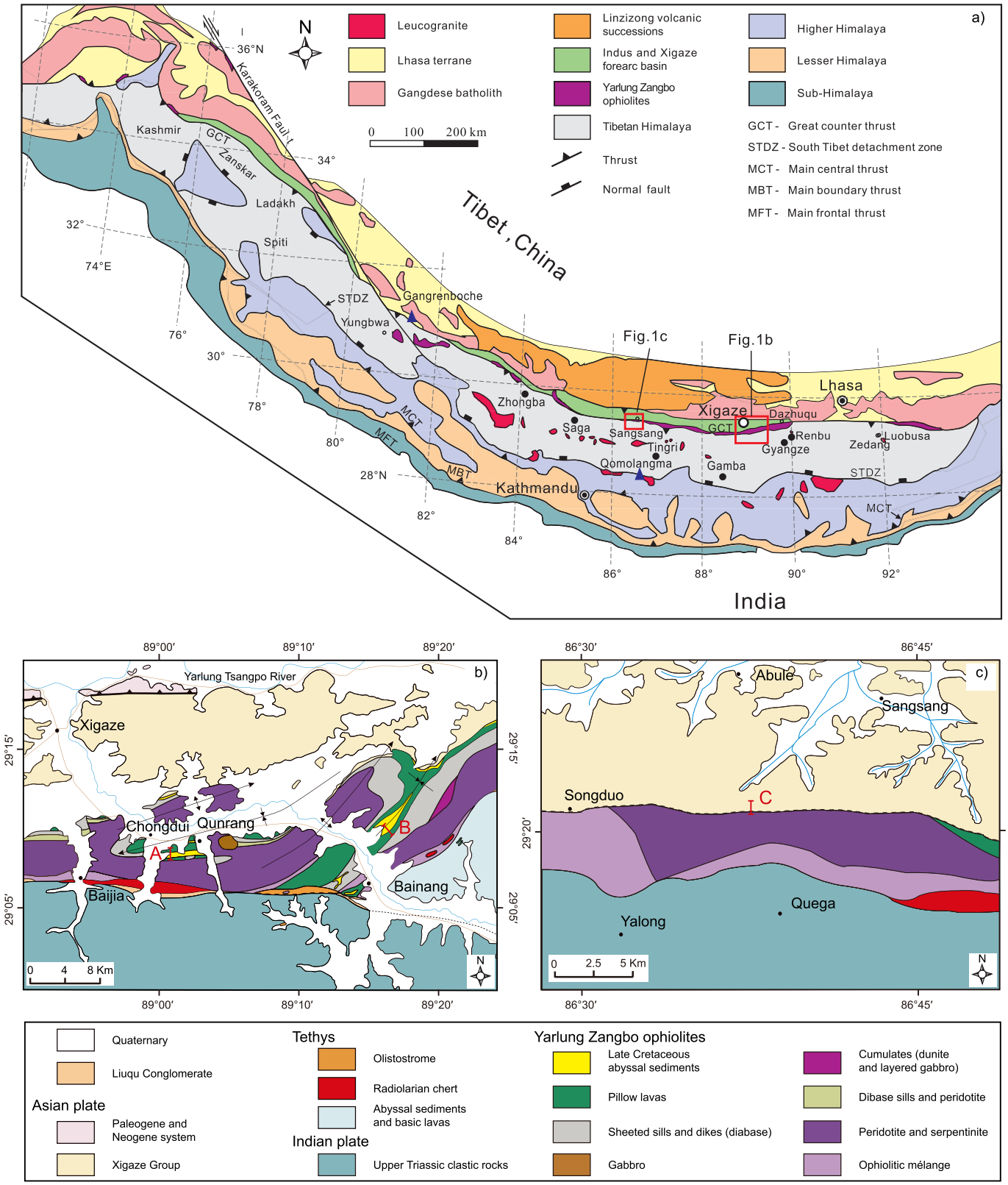

Fig. 1. (a) Simplified geological map of the Himalayas, modified from An et al. (2014). MFT: Main Frontal Thrust; MBT: Main Boundary Thrust; MCT: Main Central Thrust; STDS: Southern Tibetan Detachment System. (b) Geological map of the Xigaze ophiolite, between Xigaze and Bainang. (c) Geological map of the Xigaze ophiolite near Sangsang.

are described in Supplement A. The analytical data are reported in Table S1. We use five different methods to calculate the best age for the youngest population of zircons from these samples: (1) the peak age of the youngest distinct age group from the probability density function plot; (2) the weighted mean age calculated from the youngest cluster of ages; (3) the weighted mean age of the tightest cluster of ages determined from the *TuffZirc* algorithm, which rejects young and old ages, affected by Pb loss and inheritance, respectively; (4) the weighted mean age from the *AgePick* algorithm, which accounts for potential Pb loss and the existence

Fig. 2. Field observations of the Xigaze ophiolite and the sedimentary cover in the Chongdui, Bainang and Sangsang sections. (a–c) Depositional contact between the magmatic units (serpentinized peridotite and pillow basalt) of the Xigaze ophiolite and overlying sedimentary rocks (chert and turbidite interbedded with tuffceous sandstone layer) in Chongdui. The entire section is overturned. (d–f) Chert and turbidite overlie the pillow basalt unconformably in the Bainang section. Cherts are also found intercalated with the pillow basalt. (g–i) Serpentinized peridotites are unconformably overlain by the Cretaceous turbidite sequence in the Sangsang section.

of discrete age subpopulations by using U concentration and U/Th ratios; and (5) The mean age from the best-fitting Gaussian distribution from *Isoplots* unmixing algorithm. We find consistency amongst all five approaches, producing statistically indistinguishable ages of 116.5 ± 3.1 Ma and ∼114.1 ± 1.5 Ma, for CH-UP-1 and CH-UP-3, respectively (Figs. 3a, b).

The detrital zircon signature of sample SSH01132 primarily comprises pre-200 Ma zircons, with clusters at 500 Ma, 900–1200 Ma and 1600–1900 Ma age ranges; there are also several Archean grains present in small quantities. Fourteen grains from this sample define a youngest distinct age group in the probability density plot (Fig. 3c). Using *Isoplots* unmixing algorithm to determine the age and uncertainty of this youngest age cluster, we calculate a maximum depositional age (MDA) of 128.8 ± 3.4 Ma.

4. Paleomagnetism: methods and results

Characteristic remanent magnetizations (ChRM) were isolated using both thermal and alternating field (AF) demagnetization. Thermal cleaning was carried out in a magnetically shielded oven (ASC, model TD48-SC) for all red chert specimens ($n = 41$) from the Chongdui section, 25 selected cores from the Bainang section, and 68 cores from the Sangsang section. Thermal demagnetization was achieved through 18 steps from 200 to 685 °C. AF demagnetization was applied to all the specimens from the Bainang and Sangsang sections with an in-house developed robotized sample handler attached to a horizontal pass-through 2G Enterprises DC SQUID magnetometer (noise level 1–2 × 10^{-12} A m^2) hosted in the magnetically shielded room of the Fort Hoofddijk Paleomagnetic Laboratory, Utrecht University (Netherlands). Samples were progressively demagnetized through 17 AF steps from 5 to 100 mT.

AF and thermal demagnetization diagrams from twin specimens from the same core are comparable, although thermal demagnetization results are generally more erratic. Thermal demagnetization resulted to be an effective cleaning treatment for the red cherts of the Chongdui section. Remanence components were isolated using principal component analysis (PCA) (Fig. 4). Two components of magnetization were identified in most samples. The low stability components were commonly removed at 250–300 °C, or ∼20 mT. Well resolved ChRMs were obtained from at least five successive steps, were isolated in the interval 400–620 °C for the red cherts of the Chongdui section (Figs. 4a–c), and between 25–80 mT and 240–550 °C in the Bainang section (Figs. 4d–f), and between 20–80 mT and 280–520 °C in the Sangsang section (Figs. 4g, h, k, l). In ∼20% of the Bainang samples, and ∼50% of the Sangsang samples where a secondary component could not be entirely removed during demagnetizations, the ChRMs were determined using the great circle approach (Figs. 4i, j). Only the best resolved ChRMs characterized by a maximum angular deviation (MAD) < 15° were considered for further analysis (Table S2). These directions were additionally filtered using a fixed 45° cutoff before calculating the site mean directions.

All the isolated ChRMs have a normal polarity, which is consistent with a primary remanence acquired during the Cretaceous Normal Superchron (Gradstein et al., 2012). Site mean directions

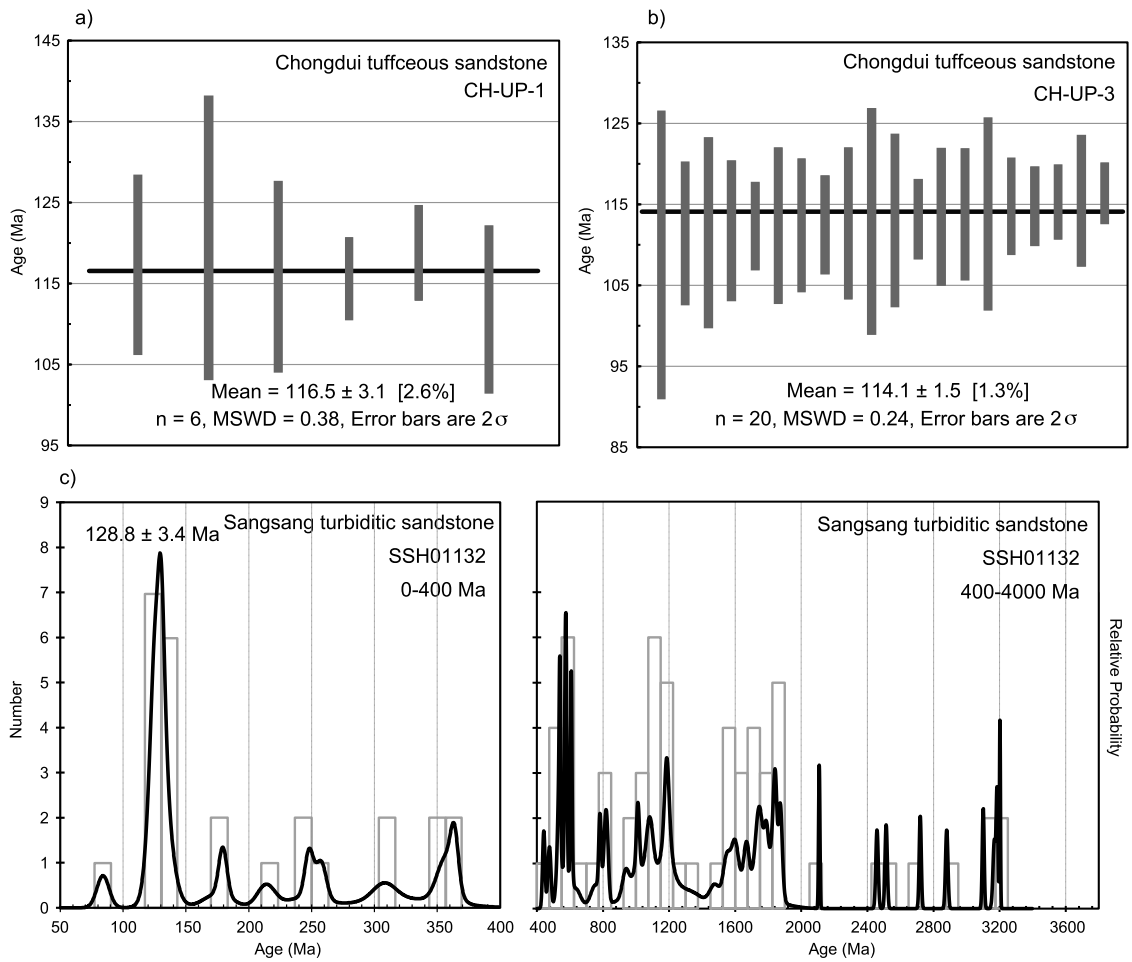

Fig. 3. U–Pb zircon dating of the collected tuff samples (a: CH-UP-1; b: CH-UP-3) from the Chongdui section and U–Pb detrital zircon dating of the sandstone sample (c: SSH01132) from the Sangsang section. Individual zircon analyses and their mean averages are presented. The plots were made using isoplot 3.60 (Ludwig, 2008).

were calculated using a Fisherian statistics of the virtual geomagnetic poles (VGPs) correspondent to the ChRMs (Deenen et al., 2011). At the Chongdui section the tilt corrected mean remanence directions resulted to have $D \pm \Delta D = 317.3 \pm 3.5°$, $I \pm \Delta I = 23.8 \pm 6.0°$ ($n = 38$, $K = 47.7$, $A_{95} = 3.4°$, $A_{95\,\mathrm{min}} = 2.8°$, $A_{95\,\mathrm{max}} = 8.3°$) (Table S2). The distribution of the ChRM directions reflects the contribution from paleosecular variation (PSV) of the geomagnetic field (i.e. A95 included between $A_{95\,\mathrm{min}}$ and $A_{95\,\mathrm{max}}$; Deenen et al., 2011). This indicates that PSV is adequately sampled in our dataset, and that both sources of scattering (i.e. tectonics) or remagnetization can be ruled out. The mean direction obtained at the Chongdui section is comparable with published data ($D \pm \Delta D = 297.1 \pm 4.8°$, $I \pm \Delta I = 15.6 \pm 8.9°$ ($n = 17$, $K = 57.8$, $A_{95} = 4.7°$) documented from the same location (GPS: 29.15505°N, 89.04503°E) by Abrajevitch et al. (2005). We therefore combined the 38 single directions from our study with the 17 directions from Abrajevitch et al. (2005), treating the latter as individual spot recordings of the magnetic field (k value of their sites are generally $\gg$100, indicating that PSV is strongly underrepresented; see Deenen et al. (2011)). The combined dataset provided a tilt corrected mean direction for the Chongdui section of $D \pm \Delta D = 310.8 \pm 3.6°$, $I \pm \Delta I = 21.6 \pm 6.4°$ ($n = 55$, $K = 30.3$, $A_{95} = 3.5°$; Fig. 5a). The clustering of the tilt corrected directions ($k = 27.8$) is much higher than the in site directions ($k = 2.1$), suggesting a pre-tilt magnetization (Figs. 6a, b). A non-parametric fold test (Tauxe and Watson, 1994) yielded a positive result (maximum clustering reached at 94–98% untilting; Fig. 6c), confirming the pre-tilt (and likely primary) origin of the remanence.

The mean tilt-corrected ChRM direction of the samples from the Bainang section is $D \pm \Delta D = 337.5 \pm 5.8°$, $I \pm \Delta I = 15.5 \pm 10.9°$ ($n = 41$, $K = 16$, $A_{95} = 5.8°$) (Figs. 5b, c). According to the Deenen et al. (2011) criteria, PSV is adequately averaged in this dataset (i.e. $A_{95\,\mathrm{min}} < A_{95} < A_{95\,\mathrm{max}}$; Table S2), excluding both within-site rotations and remagnetizations. This scatter can be explained by paleo-secular variation (for $n = 41$, $A_{95\,\mathrm{min}} = 2.7°$, $A_{95\,\mathrm{max}} = 7.9°$).

The Sangsang section yields a mean ChRM direction of $D \pm \Delta D = 351 \pm 3.6°$, $I \pm \Delta I = 16.9 \pm 6.6°$ ($n = 117$, $K = 14.6$, $A_{95} = 3.5°$, $A_{95\,\mathrm{min}} = 1.8°$, $A_{95\,\mathrm{max}} = 4.1°$) (Fig. 5c). The distribution of the ChRMs inferred from the A_{95} values indicates that the scatter is consistent with PSV, and that the magnetization was acquired during a sufficient time to average PSV. No remagnetization or internal rotations enhancing that scatter are thus likely (Deenen et al., 2011). Variable bedding attitude in the upper part of the Sangsang section, few hundred meters away from the contact with the ophiolite, allow us to perform a fold test. After tilt correction the clustering of the ChRMs increases substantially ($k_{\mathrm{in\ situ}} = 1.3$; $k_{\mathrm{tilt\ corrected}} = 10.8$) (Figs. 6d, e). The non-parametric fold test (Tauxe and Watson, 1994) yielded a positive result with best grouping reached at 99–106% untilting (Fig. 6f), indicating a pre-tilt origin of the remanence.

5. Rock magnetism and magnetic fabric

We performed rock magnetic analyses, including thermomagnetic experiments, hysteresis measurements, and component anal-

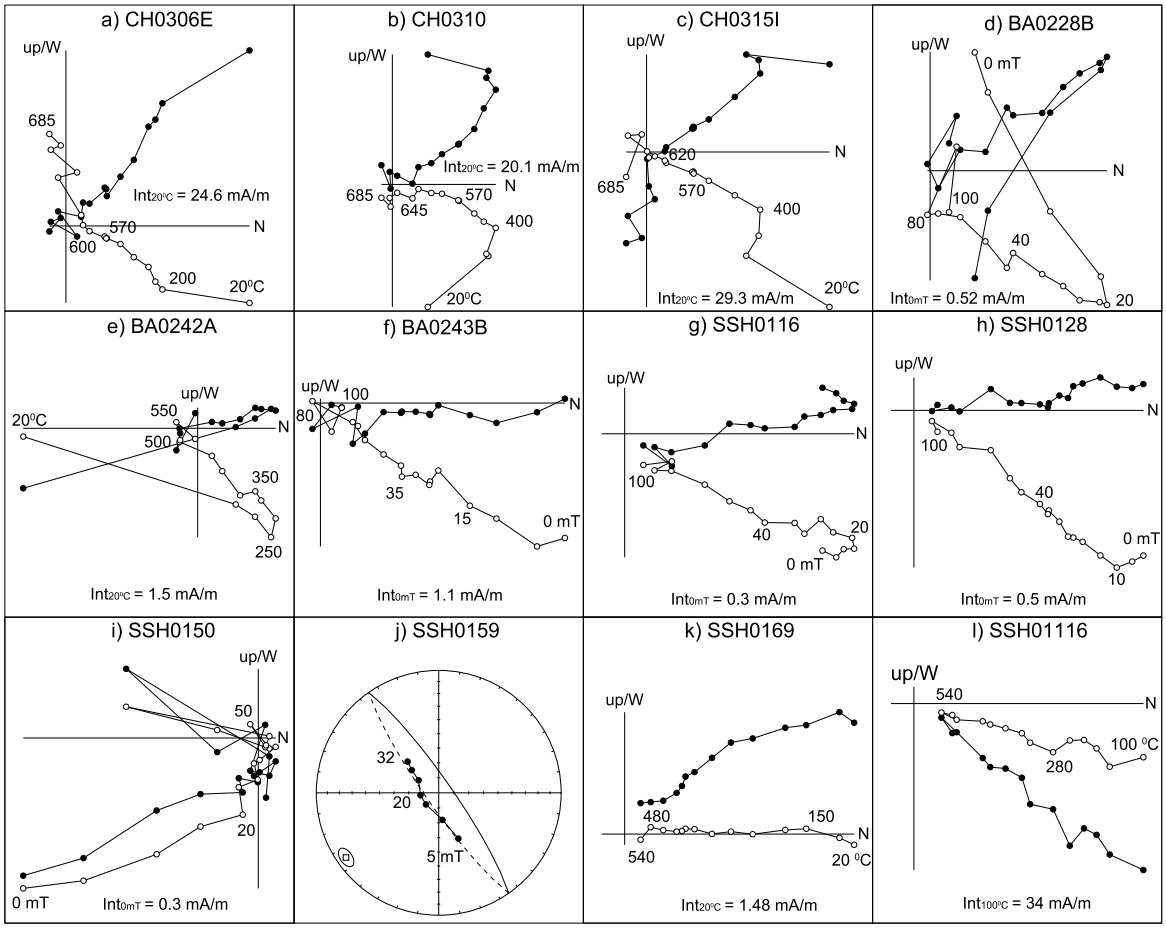

Fig. 4. Representative demagnetization diagrams for sedimentary samples from the Chongdui, Bainang and Sangsang sections. All diagrams are displayed after bedding tilt correction. Closed (open) symbols represent the projection of vector end-points on the horizontal (vertical) plane; values represent alternating field and thermal demagnetization steps in mT (millitesla) and °C, respectively.

ysis of the isothermal remanent magnetization (IRM) (Kruiver et al., 2001), to identify the magnetic carrier(s) of the studied rocks. Magnetic fabric of the sandstones from the Sangsang section was also investigated with anisotropy of magnetic susceptibility (AMS) and anisotropy of anhysteretic remanent magnetization (AARM) measurements to allow inclination shallowing corrections. Detailed description of the methods is presented in Supplement B.

5.1. Thermomagnetic curves, hysteresis loops and IRM component analysis

Magnetization variation during temperature increase in the red chert samples from the Chongdui section show a progressive, quasi-reversible decrease up to ∼620 °C, followed by a more rapid decrease up to 680 °C (Fig. 7a). The hysteresis loops are wasp-waisted and not fully saturated at maximum fields of 1 T (Fig. 7b), indicating a mixture of low and high coercivity magnetic minerals (Roberts et al., 1995). The B_c and B_{cr} values are also very high (Table S3). The analysis of the IRM acquisition curves (Kruiver et al., 2001) show the presence of two magnetic phases contributing to the remanence: mainly hematite, with minor occurrence of magnetite (Fig. 7c; Table S4).

For the greenish cherts from the Bainang section, the hyperbolic shape of the thermomagnetic curves is indicative of a dominant paramagnetic fraction component contribution (Fig. 7d). All the analyzed samples show an irreversible decrease of magnetization up to ∼580 °C (Curie temperature of magnetite). The hysteresis loops are narrow and essentially saturated at 500 mT (Fig. 7e). The B_c and B_{cr} values are also low, indicating a dominant low-coercivity component (Table S3). The fitting of the IRM acquisition curves are characterized by components 1 and 2 (Fig. 7f), indicating the predominace of magnetite in the rocks from the Bainang section.

Rapid decay of magnetization in the range of 520–580 °C (Figs. 7g, j), saturation of the magnetization at ∼500 mT (Figs. 7h, k), and the IRM component analysis (Figs. 7i, l) consistently indicated the main occurrence of magnetite in all samples from the Sangsang section. Two sub-groups of samples can, however, be recognized: a first sub-group characterized by an increase in magnetization above ∼430 °C (Fig. 7g), likely due to the breakdown of iron sulphides into magnetite; and a second sub-group showing minor contribution of hematite, likely produced by weathering (Fig. 7l).

5.2. Magnetic fabric

Magnetic susceptibility of the Sangsang section varies from 7.8×10^{-5} SI to 4.1×10^{-4} SI. AMS and AARM measurements yielded consistent results, and showed a magnetic fabric characterized by both prolate and oblate ellipsoids (Figs. S1a, d; Tables S5, S6). The anisotropy degree values (P) range from 1.006 to 1.034, with a mean of 1.018 (Fig. S1a; Table S5). The AARM analysis, however, yielded much higher P values, ranging from 1.030 to 1.261 with a mean value of 1.116 (Fig. S1d; Table S6).

The in situ K_{max} axes if both AMS and AARM show a consistent near E–W orientation (Figs. S1c, g) that is parallel to the regional strike of the Sangsang section (i.e. 265°N), thus suggesting ∼N–S

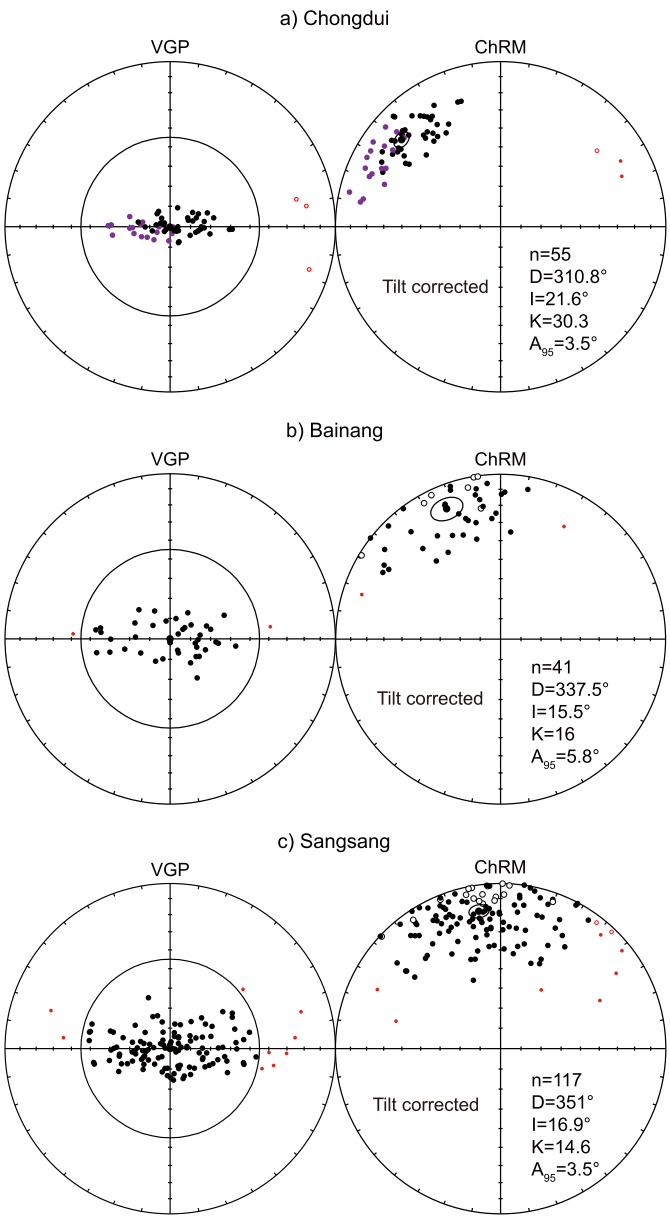

Fig. 5. (a) VGPs (left) and equal-area projections (right) of the isolated ChRM directions from red cherts of the Chongdui section in stratigraphic coordinates. Red dots (circles) are rejected by the 45° cut-off criterion (Deenen et al., 2011). Purple dots are results from cherts and mudstones in a similar section reported by Abrajevitch et al. (2005). Large circles represent mean ChRM directions and 95% confidence limit. (b) Same plots for the green cherts in the Bainang section. (c) Same plots for the turbiditic sandstones in the Sangsang section.

shortening. After tilt correction, $K_{\min}$ axes cluster near the vertical with $K_{\max}$ and K_{int} axes being dispersed on the horizontal plane (Figs. S1d, h), indicating that the magnetic fabric is also related to depositional compaction.

6. Inclination shallowing correction

The plaeomagnetic inclination shallowing effect has been frequently documented in clastic sedimentary rocks (e.g., Jackson et al., 1991). The two most common methods used to perform this correction are based on the elongation/inclination (E/I) correction of the ChRM distribution (Tauxe and Kent, 2004), and the anisotropy of susceptibility or remanence (Jackson et al., 1991; Tan et al., 2003; Bilardello and Kodama, 2009; Kodama, 2009). Comparative studies show that these two methods provide correction values that are comparable within error (e.g., Huang et al., 2013). We applied both methods for the correction of the inclination shallowing affecting the sandstones in Sangsang section, which is indicated by the strong ellipsoid distribution of the VPGs (Fig. 5c), as well as the well-developed magnetic fabric described above (Fig. S1).

6.1. Elongation/inclination (E/I) correction

The E/I correction is based on the statistical paleosecular variation models of the geocentric axial dipole magnetic field (Tauxe and Kent, 2004). After application of the E/I method on the dataset of the Sangsang sandstones, the mean inclination is corrected from $16.9 \pm 6.6°$ to 30.2° with 95% confidence limits between 24.8° and 37.3° (Fig. 8a). This significant correction further indicates that the ChRMs of the Sangsang sandstone do have a primary origin (i.e., it has been acquired during or shortly after the deposition and was subsequently fattened). A further estimate of the mechanism of remanence acquisition for the Sangsang sandstones based on end-member modeling of IRM acquisition curves (Gong et al., 2009) can be seen in Supplement C and Fig. S2. It is unlikely that the remanence isolated from Sangsang sandstones is induced by widespread remagnetization events in southern Tibet (e.g., Huang et al., 2014, 2015).

6.2. Anisotropy-based inclination correction

For the anisotropy-based method, the bulk anisotropies can be AMS, AARM (for magnetite), or high-field anisotropy of IRM (hf-AIR, for hematite). Individual magnetic particle anisotropy can be measured directly using specialized laboratory equipment (e.g., Kodama, 1997); it can also be determined by least-squares curve fitting of AMS, AARM (for magnetite) and AIR (for hematite) data (Tan et al., 2003; Bilardello and Kodama, 2009; Kodama, 2009). Our rock magnetic analyses and results of end-member modeling have indicated that magnetite is the dominant magnetic carrier in the Sangsang section. We therefore use the simplified method of Kodama (2009) to estimate the individual particle anisotropy of the magnetite in the Sangsang sandstone.

The theoretical expression to describe the particle anisotropy of magnetite is:

$$\tan I_o / \tan I_c = \left[K_{\min}(a+2) - 1\right] / \left[K_{\max}(a+2) - 1\right], \quad (1)$$

where I_c is the corrected inclination, $K_{\min}$ and $K_{\max}$ are the maximum and minimum normalized eigenvalues, respectively and a is the individual particle anisotropy, which can be either a_γ (for remanence) or a_χ (for susceptibility). In effect, a_γ and a_χ are estimated with a least-squares fit of the sample AARMs and AMS to the theoretical anisotropy expression. Details of this method can be found in Kodama (2009). In the least-squares fit, the root mean square (rms) error decreases monotonically with decreasing values of a_γ (Fig. 8b). The critical value of $a_\gamma = 1.40$ is reached when theoretical values calculated from the right-hand side of Eq. (1) using lower a_γ values become negative for at least one sample in the data set. Individual particle anisotropies lower than 1.40 will make $[K_{\min}(a_\gamma + 2) - 1] < 0$ for samples having a lower $K_{\min}$, which is incompatible with the range of measured anisotropies for these samples (Kodama, 2009). When we applied the curve fitting to our AMS dataset, no meaningful a_χ could be determined. This is probably caused by the strong contribution of paramagnetic/diamagnetic minerals to the measured AMS (Kodama, 2009; Huang et al., 2013). This estimated $a_\gamma = 1.40$ is actually similar to the $a_\gamma = 1.39$ determined by the same approach on the volcaniclastic rocks of the Linzizong Group in the southern Tibet

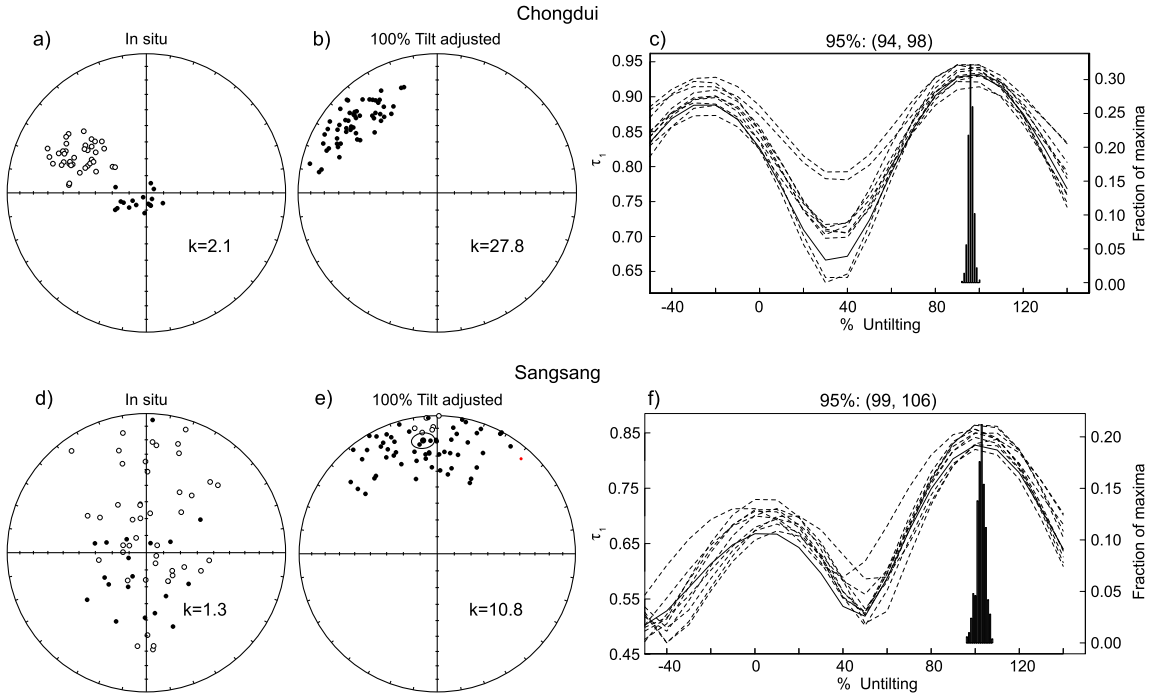

Fig. 6. (a–c) Non-parametric fold test (Tauxe and Watson, 1994) on the samples from the Chongdui section after combining the results of Abrajevitch et al. (2005). Equal-area plots of the individual ChRM directions from each specimen in geographic coordinates (a) and after tilt correction (b). Before tilt correction, the ChRM directions of samples are in two different groups. After tilt correction, the two groups cluster together. Results of the fold test with bootstrapped statistics on the first eigenvalues (τ_1) upon progressive untilting. The 95% bootstrap error interval is indicated. Best grouping is reached at 94–98% untilting. (d–f) Similar non-parametric fold test (Tauxe and Watson, 1994) on the samples from the Sangsang section. Before tilt correction, the ChRM directions are scattered. After tilt correction, they are clustered. Results of the fold test with bootstrapped statistics on the first eigenvalues (τ_1) upon progressive untilting. The 95% bootstrap error interval is indicated. Best grouping is reached at 99–106% untilting.

(Huang et al., 2013). After application of $a_\gamma = 1.40$ to the ChRM determined from the Sangsang sandstones, we calculated a mean direction of $D = 350.7°$, $I = 31.1°$ ($n = 64$, $K = 9.8$, $A_{95} = 6°$) (Fig. 8b). This direction is statistically indistinguishable from the corrected direction by the E/I method.

7. Discussion

7.1. Where did the Xigaze ophiolite form?

In this study, we investigated three sedimentary sections that overlie the Xigaze ophiolite. Our new zircon U–Pb geochronologic results provide a maximum depositional age of the sedimentary rocks at Sangsang of ∼129 Ma (base of the Sangsang section) and the depositional age of the Chongdui section of ∼116–114 Ma. These ages are consistent with previous radiolarian biostratigraphic studies (Ziabrev et al., 2003) and detrital zircon U–Pb dating results from the Xigaze Group turbiditic sandstones (Wu et al., 2010), and overlap with the ages of the magmatic units of the Xigaze ophiolite of ∼130–120 Ma (e.g., Guilmette et al., 2009; Dai et al., 2013). The radiolarites of the Chongdui section that overlie the pillow lavas, interfinger with sandy turbidites that were previously ascribed to the Xigaze forearc (e.g., Wu et al., 2010). The U–Pb age spectrum obtained from the basal sandstone in the Sangsang section of the Xigaze Group is consistent with derivation from the Lhasa terrane, which is in agreement with the study of the Xigaze forearc basin's basal sediments published in An et al. (2014). Moreover, the unconformable contact of these deep-marine strata with the underlying serpentinized peridotites and the age consistency between the ophiolites and the basal Sangsang sandstone suggest that the Xigaze Group was deposited onto mantle rocks that were exhumed to the sea floor, perhaps along an oceanic detachment fault immediately before deposition (Maffione et al., submitted for publication). This unconformable contact thus allows us to constrain the paleolatitude of the spreading of the Xigaze ophiolite through paleomagnetic study of their sedimentary cover.

The paleolatitude inferred for the Xigaze ophiolite by Pozzi et al. (1984) was only based on one site (radiolarites; $n = 14$) near Chongdui and one site (limestones; $n = 9$) from the Xigaze Group, and were used to calculated a paleolatitude of 10–20°N. Given modern statistical criteria (Deenen et al., 2011), these datasets are quite small to define a reliable paleolatitude, and certainly too small to test for inclination shallowing. Our paleomagnetic results of the Chongdui section are comparable to results from cherts and mudstones in a section of similar age reported by Abrajevitch et al. (2005) near Qunrang (Fig. 1b), and combined datasets yield an inclination that would suggest a paleolatitude of 11.2°N [7.7°N, 14.9°N]. We cannot apply neither the E/I method (Tauxe and Kent, 2004), nor the anisotropy-based correction method (Tan et al., 2003; Bilardello and Kodama, 2009) to assess the magnitude of inclination shallowing in these rocks due to the limited number of isolated ChRM directions and the unavailability of magnetic fabric data. The strongly elongated distribution of the VGPs (Fig. 5a), however, is a firm indication that inclination flattening has played a significant role. Our paleomagnetic results from the Chongdui section, including those from Abrajevitch et al. (2005), should be treated as a minimum value for the inclination and paleolatitude. We observe a similar elongated distribution of the VGPs from the cherts from the Bainang section (Fig. 5b), indicating that inclination shallowing is likely a fundamental problem in radiolarian cherts, as previously shown by Collombat et al. (1993). These paleomagnetic results, without correcting the shallowing bias, should therefore not be used for paleolatitude studies.

Our geochronological, paleomagnetic and rock magnetic studies on the sandstones from the Sangsang section demonstrate their immediate deposition above the Xigaze ophiolite, the primary origin of the remanence and the existence of the inclination shallowing of the remanence. The applied E/I method has yielded a

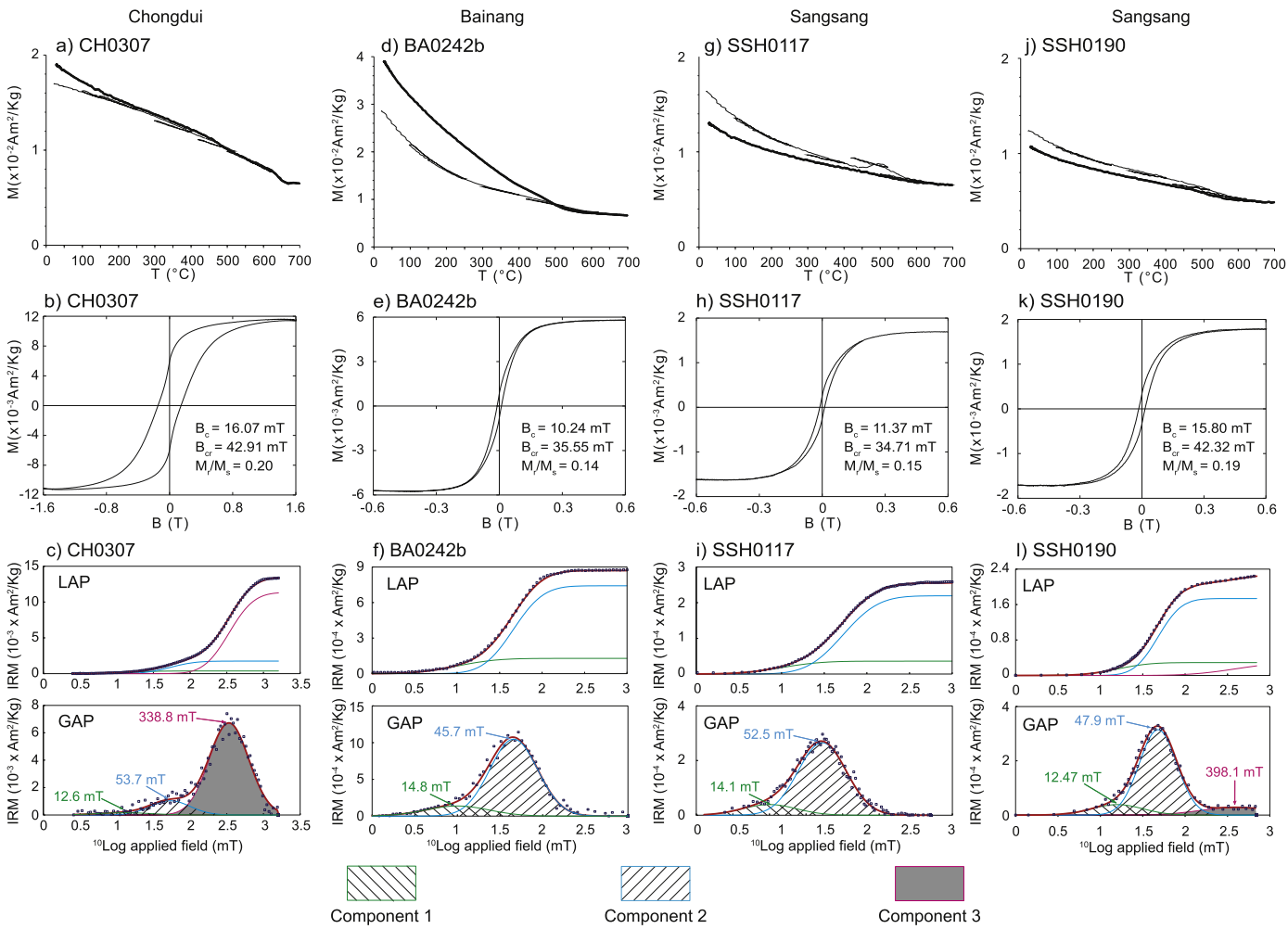

Fig. 7. Typical rock magnetic results of red chert samples from the Chongdui section (a–c), green chert samples from the Bainang section (d–f) and sandstone samples from the Sangsang section (g–l). For each group, a representative high-field thermomagnetic run with thin (thick) lines representing the heating (cooling) curves; hysteresis loop, and IRM component analysis results are shown. Methodological descriptions of the analyses can be found in Supplement B. IRM component analysis was applied following Kruiver et al. (2001). Three components are required to fit the IRM acquisition curves: component 1 with very low $B_{1/2}$ (the field at which half of saturation isothermal remanent magnetization (SIRM) is reached) of ∼10 mT and dispersion parameter (DP) of ∼0.30 (log units) is interpreted to be thermally activated component 2 particles; component 2 with $B_{1/2}$ of ∼55 mT and DP of ∼0.30 typically represents magnetite; component 3 has high $B_{1/2}$ of ∼340 mT and is interpreted to represent hematite.

corrected mean inclination of 30.2° [24.8°, 37.3°] (Fig. 8a), corresponding to a paleolatitude of 16.2°N [13°N, 20.9°N]. This is indistinguishable from the AARM-based correction, yielding a mean inclination of 31.1° ± 9.6° (Fig. 8b), corresponding to a paleolatitude of 16.8°N [11.1°N, 23.3°N]. These corrected paleolatitudes values are both statistically indistinguishable from the Early Cretaceous (∼120 Ma) paleolatitudes of the Lhasa terrane of 14.7 ± 5.5°N and 18.6 ± 2.1°N (Fig. 9; Table S7), determined from 30 and 51 lava sites, respectively (Chen et al., 2012; Ma et al., 2014; Yang et al., 2014). Together with U–Pb detrital zircon age spectrum of the sandstone unconformably covering the Sangsang serpentinized peridotites, our paleomagnetic data demonstrate that the Xigaze ophiolite formed immediately adjacent to the Lhasa terrane in the forearc of the Gangdese arc.

Constraining the original N–S dimension of the oceanic forearc of the Gangdese arc is beyond the accuracy of paleomagnetism. It was previously noted that the Gangdese volcanic arc is presently located along the southern margin of the Lhasa terrane, immediately adjacent to the suture, suggesting that significant shortening of the forearc must have occurred (e.g., Yin et al., 1999; van Hinsbergen et al., 2011). Typical forearc dimensions today are 166 ± 60 km, which is well within the paleomagnetic error bars of our analysis. The removal of this forearc by shortening likely occurred upon collision of the Tibetan Himalaya with the Xigaze forearc (i.e. along the Gangdese thrust (Yin et al., 1999)), and the obduction of the forearc basement (i.e. the Xigaze ophiolite) onto the Tibetan Himalaya. Previous paleomagnetic analyses argue for an initial collision of the Tibetan Himalaya and the Lhasa terrane by 49.5 ± 4.5 Ma, using the paleolatitude of the southern Lhasa margin as marker (e.g., Dupont-Nivet et al., 2010a; van Hinsbergen et al., 2012; Lippert et al., 2014), consistent with stratigraphic studies (e.g., Najman et al., 2010). Adding the original N–S width of the forearc will shift this timing of collision to 52 ± 5 Ma (Lippert et al., 2014), in line with recent stratigraphic studies arguing for a collision around 58–56 Ma (DeCelles et al., 2014; Garzanti and Hu, 2014; Orme et al., 2014).

7.2. Implications for intra-oceanic subduction within the Neotethys

The previous paleomagnetic arguments of Abrajevitch et al. (2005) for a near-equatorial supra-subduction zone derivation of the Xigaze ophiolite is supported by seismic tomographic images of subducted lithosphere below the Indian plate, where high-velocity mantle anomalies appear to exist at equatorial latitudes (e.g., anomaly III of Van der Voo et al. (1999), see also van Hinsbergen et al. (2012)). In the light of Abrajevitch et al. (2005), the Xigaze ophiolite was previously taken as geological evidence

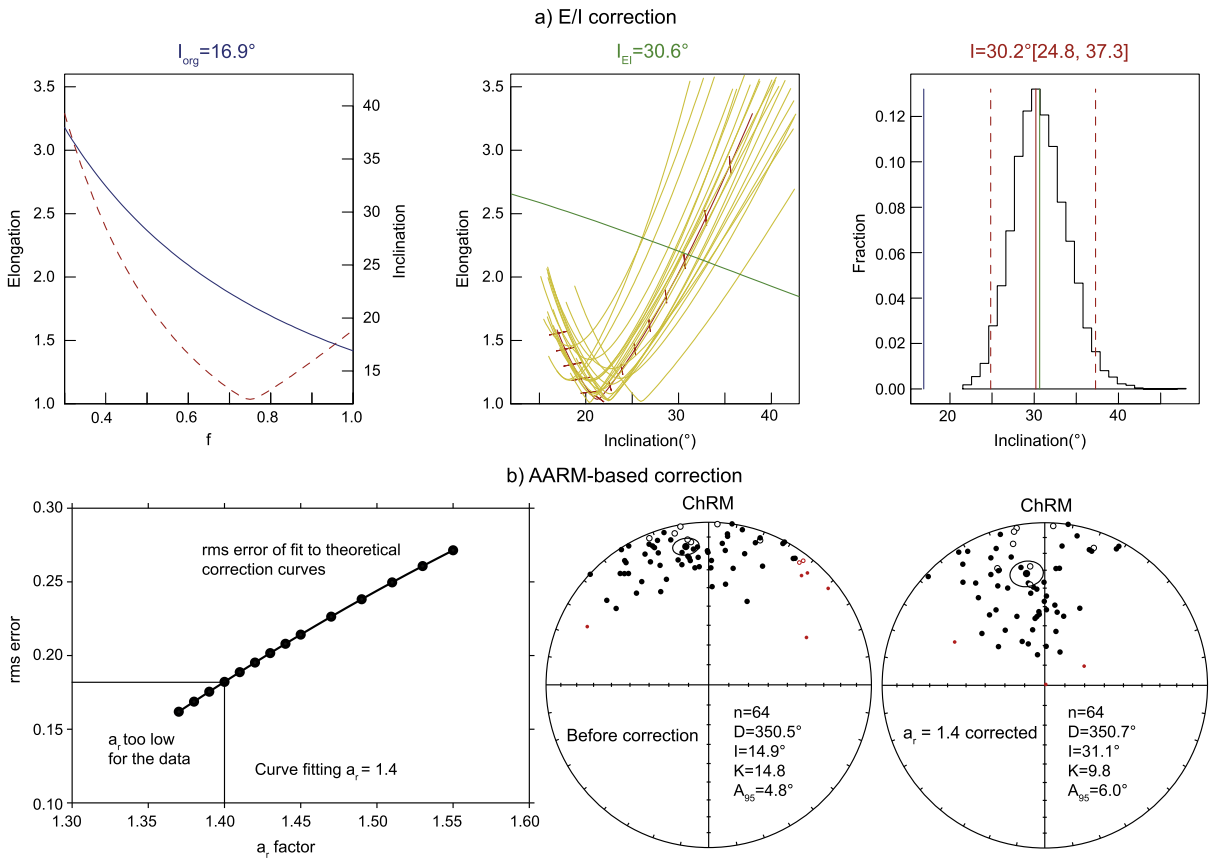

Fig. 8. Inclination shallowing corrections of the sandstones in the Sangsang section based on two methods. (a) Correction for the inclination error using the E/I method developed by Tauxe and Kent (2004). Plot of elongation versus inclination for the TK03.GAD model shown on left, where the dashed curve shows the variation of the elongation of the data set distribution with respect to mean inclination when affected by flattening factor ranging from 0.3 to 1; barded line in the central panel is the range of elongation–inclination obtained upon applying a range of flattening factors (King, 1955) on the original data set. Right-hand fraction/inclination plot indicate the distribution of the corrected inclinations with 95 percent confidence limit. (b) AARM-based correction. Left: least-squares curve fitting of sample AARM data to the theoretical inclination correction curves for magnetite (Jackson et al., 1991; Kodama, 2009) for the 64 ChRM directions and their measured AARM anisotropies of the Sangsang sandstones. The rms error decreases until $a_\gamma = 1.40$. Smaller values of a_γ are inconsistent with the AARM data (see text). The lowest rms error therefore occurs at $a_\gamma = 1.40$; Middle and right: equal-area projections of the 64 individual ChRM directions before and after correction with $a_\gamma = 1.40$.

for the existence of a northward dipping equatorial intra-oceanic subduction zone and island arc system within Neotethys (e.g., Abrajevitch et al., 2005; Hébert et al., 2012; van Hinsbergen et al., 2012). Our results, however, demonstrate that the Xigaze ophiolite can no longer be viewed as a geological archive of near-equatorial subduction within the Neotethys. Additional support for a near-equatorial ophiolite emplacement onto the Tibetan Himalaya was previously inferred from the arrival of mafic magmatic debris in the Maastrichtian–Paleocene stratigraphy of the Tibetan Himalaya (e.g., Ding et al., 2005), but we note that recent provenance analysis suggests that this debris was not derived from ophiolites, but from hotspot-related volcanic rocks instead (Garzanti and Hu, 2014).

Our study does not necessarily argue against intra-oceanic subduction within the Neotethys, but we conclude that the evidence from the Xigaze ophiolite cannot be used to support its former existence. Geochemical studies have indicated a variety of compositions and geochemically inferred geodynamic settings in the Yarlung Zangbo ophiolite belt (Hébert et al., 2012). Our paleomagnetic results, as well as the stratigraphic and sedimentary evolution of the Xigaze ophiolite's cover presented in An et al. (2014), suggest that this geochemical complexity should somehow have evolved during the extensional fragmentation of the Gangdese forearc that culminated in the formation of the Xigaze ophiolite, and led to their dismemberment (see also Dai et al., 2013; Maffione et al., submitted for publication).

8. Conclusion

Our study based on stratigraphy and sedimentary provenance confirms a depositional contact between the Xigaze ophiolite and the overlying forearc sedimentary rocks from the Xigaze Group. The oldest depositional age of the sedimentary cover with Lhasa provenance was dated at ∼129–114 Ma. New paleomagnetic data, after correction of the inclination shallow bias of the sedimentary rocks, yielded a robust paleolatitude of the Xigaze ophiolite at ∼16.5°N.

The Xigaze ophiolite demarcates the India–Asia suture zone and exposes Lower Cretaceous ophiolites and radiolarian cherts, and time-equivalent Asia-derived clastic forearc sediments (Xigaze Group). These ophiolites, frequently in tectonic contact with the forearc sediments, were previously interpreted as either formed in the forearc of the subduction zone below Tibet that produced the Gangdese arc around 15–20°N, or, alternatively, in the forearc of a sub-equatorial intra-oceanic subduction zone. Our study based on stratigraphy and sedimentary provenance demonstrates that the Xigaze group turbiditic sandstones, with a maximum depositional age of 128.8 ± 3.4 Ma, are in unconformable contact with serpentinized peridotites exhumed to the sea floor in the Sangsang ophiolite. In addition, Xigaze Group turbidites interfinger with radiolarian cherts and tuffaceous sandstones (maximum depositional ages of 116.5 ± 3.1 Ma and 114 ± 1.5 Ma) in the Chongdui section on the Xigaze ophiolite. We present pa-

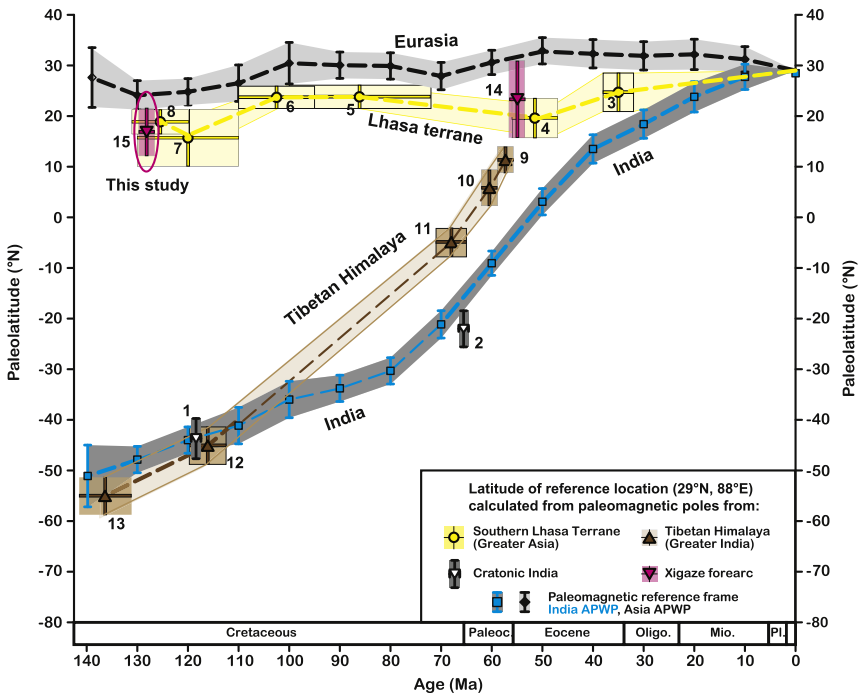

Fig. 9. Paleolatitudes of a reference site (29°N, 88°E) located on the present-day position of the Yarlung Zangbo suture zone in Eurasian, Greater Asian, Tibetan–Himalayan, and Indian reference frames (modified from van Hinsbergen et al., 2012). Numbers correspond to paleomagnetic poles described and listed in Table S7. Pl., Pliocene; Mio., Miocene; Oligo., Oligocene; Paleoc., Paleocene. Age uncertainties are based on the age of the units determined from either radiometric dates or geologic stages, and latitude uncertainties are calculated from the corresponding poles at the 95% confidence level. See Table S7 for details. Paleolatitude of the Xigaze ophiolite overlaps with the early Cretaceous paleolatitudes of the Lhasa terrane.

leomagnetic data that after correction of the inclination shallow bias of the sedimentary rocks, yield a robust paleolatitude of the Xigaze ophiolite at 16.2°N [13°N, 20.9°N] and 16.8°N [11.1°N, 23.3°N] (based on two shallowing correction methods), statistically indistinguishable from time-equivalent paleolatitudes of the Gangdese arc of southern Tibet. Our new data show that the previous evidence for an apparent sub-equatorial formation latitude of the Xigaze ophiolite resulted from compaction-induced inclination shallowing. Thereby, conclusive geological evidence for a the widely-accepted, Cretaceous intra-oceanic subduction and island arc system within the Neotethys between India and Asia, which may find support in seismic tomographic studies, remains to be found.

Acknowledgements

This work was funded by the U.S. NSF Continental Dynamics grant EAR-1008527 'The Suturing Process: Insight from the India–Asia collision zone', the Netherlands Organisation for Scientific Research (NWO) with VIDI grants to G.D.-N. and D.J.J.v.H., the European Research Council (ERC) Starting Grant number 306810 (SINK) to D.J.J.v.H., the Alexander von Humboldt Foundation grant to G.D.-N., and the Cai Yuanpei program of the French Ministry of Foreign Affairs and Ministry of Higher Education and Research, and the Ministry of Education of the People's Republic of China. We thank Pierrick Roperch for lab assistance, Xiao Wang and Shun Li for field assistance. We are grateful to Xiumian Hu, an anonymous reviewer, and the Editor An Yin for their constructive comments and suggestions.

Appendix A. Supplementary material

Supplementary material related to this article can be found online at http://dx.doi.org/10.1016/j.epsl.2015.01.032.

References

Abrajevitch, A.V., Ali, J.R., Aitchison, J.C., Davis, A.M., Liu, J., Ziabrev, S.V., 2005. Neotethys and the India–Asia collision: insights from a palaeomagnetic study of the Dazhuqu ophiolite, southern Tibet. Earth Planet. Sci. Lett. 233, 87–102.

Aitchison, J.C., Davis, A.M., Abrajevitch, A.V., Ali, J.R., Liu, J., Luo, H., McDermid, I.R., Ziabrev, S.V., 2003. Stratigraphic and sedimentological constraints on the age and tectonic evolution of the Neotethyan ophiolites along the Yarlung Tsangpo suture zone, Tibet. Geol. Soc. (Lond.) Spec. Publ. 218, 147–164.

Aitchison, J.C., Ali, J.R., Davis, A.M., 2007. When and where did India and Asia collide? J. Geophys. Res., Solid Earth 112, B05423. http://dx.doi.org/10.1029/2006JB004706.

An, W., Hu, X., Garzanti, E., BouDagher-Fadel, M.K., Wang, J., Sun, G., 2014. Xigaze forearc basin revisited (South Tibet): provenance changes and origin of the Xigaze ophiolite. Bull. Geol. Soc. Am. 126, 1595–1613.

Bilardello, D., Kodama, K.P., 2009. Measuring remanence anisotropy of hematite in red beds: anisotropy of high-field isothermal remanence magnetization (hf-AIR). Geophys. J. Int. 178, 1260–1272.

Chen, W., Yang, T., Zhang, S., Yang, Z., Li, H., Wu, H., Zhang, J., Ma, Y., Cai, F., 2012. Paleomagnetic results from the Early Cretaceous Zenong Group volcanic rocks, Cuoqin, Tibet, and their paleogeographic implications. Gondwana Res. 22, 461–469.

Collombat, H., Rochette, P., Kent, D.V., 1993. Detection and correction of inclination shallowing in deep sea sediments using the anisotropy of an hysteretic remanence. Bull. Soc. Geol. France 164, 103.

Corfield, R.I., Searle, M.P., Pedersen, R.B., 2001. Tectonic setting, origin, and obduction history of the Spontang Ophiolite, Ladakh Himalaya, NW India. J. Geol. 109, 715–736.

Dai, J., Wang, C., Polat, A., Santosh, M., Li, Y., Ge, Y., 2013. Rapid forearc spreading between 130 and 120 Ma: evidence from geochronology and geochemistry of the Xigaze ophiolite, southern Tibet. Lithos 172, 1–16.

DeCelles, P., Kapp, P., Gehrels, G., Ding, L., 2014. Paleocene–Eocene foreland basin evolution in the Himalaya of southern Tibet and Nepal: Implications for the age of initial India–Asia collision. Tectonics 33, 824–849. http://dx.doi.org/10.1002/2014TC003522.

Deenen, M.H.L., Langereis, C.G., van Hinsbergen, D.J.J., Biggin, A.J., 2011. Geomagnetic secular variation and the statistics of paleomagnetic directions. Geophys. J. Int. 186, 509–520.

Ding, L., Kapp, P., Wan, X., 2005. Paleocene–Eocene record of ophiolite obduction and initial India–Asia collision, south central Tibet. Tectonics 24, TC3001. http://dx.doi.org/10.1029/2004TC001729.

Dupont-Nivet, G., Lippert, P.C., van Hinsbergen, D.J.J., Meijers, M.J.M., Kapp, P., 2010a. Palaeolatitude and age of the Indo–Asia collision: palaeomagnetic constraints. Geophys. J. Int. 182, 1189–1198.

Dupont-Nivet, G., van Hinsbergen, D.J.J., Torsvik, T.H., 2010b. Persistently low Asian paleolatitudes: implications for the India–Asia collision history. Tectonics 29, TC5016. http://dx.doi.org/10.1029/2008TC002437.

Garzanti, E., Hu, X., 2014. Latest Cretaceous Himalayan tectonics: obduction, collison or deccan-related uplift? Gondwana Res.. http://dx.doi.org/10.1016/j.gr.2014.1003.1010.

Gong, Z., Dekkers, M., Heslop, D., Mullender, T., 2009. End-member modelling of isothermal remanent magnetization (IRM) acquisition curves: a novel approach to diagnose remagnetization. Geophys. J. Int. 178, 693–701.

Gradstein, F.M., Ogg, J.G., Schmitz, M., Ogg, G., 2012. The Geologic Time Scale 2012. Cambridge University Press, Cambridge.

Guilmette, C., Hébert, R., Wang, C., Villeneuve, M., 2009. Geochemistry and geochronology of the metamorphic sole underlying the Xigaze ophiolite, Yarlung Zangbo Suture Zone, south Tibet. Lithos 112, 149–162.

He, S., Kapp, P., DeCelles, P.G., Gehrels, G.E., Heizler, M., 2007. Cretaceous–Tertiary geology of the Gangdese Arc in the Linzhou area, southern Tibet. Tectonophysics 433, 15–37.

Hébert, R., Bezard, R., Guilmette, C., Dostal, J., Wang, C., Liu, Z., 2012. The Indus–Yarlung Zangbo ophiolites from Nanga Parbat to Namche Barwa syntaxes, southern Tibet: first synthesis of petrology, geochemistry, and geochronology with incidences on geodynamic reconstructions of Neo-Tethys. Gondwana Res. 22, 377–397.

Hu, X., An, W., Wang, J., Garzanti, E., Guo, R., 2014. Himalayan detrital chromian spinels and timing of Indus–Yarlung ophiolite erosion. Tectonophysics 621, 60–68.

Huang, W., Dupont-Nivet, G., Lippert, P.C., van Hinsbergen, D.J., Hallot, E., 2013. Inclination shallowing in Eocene Linzizong sedimentary rocks from Southern Tibet: correction, possible causes and implications for reconstructing the India–Asia collision. Geophys. J. Int. 194, 1390–1411.

Huang, W., van Hinsbergen, D.J.J., Dekkers, M.J., Garzanti, E., Dupont-Nivet, G., Lippert, P.C., Li, X., Maffione, M., Langereis, C.G., Hu, X., Guo, Z., Kapp, P., 2014. Paleolatitudes of the Tibetan Himalaya from primary and secondary magnetizations of Jurassic to Lower Cretaceous sedimentary rocks. Geochem. Geophys. Geosyst. 16. http://dx.doi.org/10.1002/2014GC005624.

Huang, W., Dupont-Nivet, G., Lippert, P.C., van Hinsbergen, D.J.J., Dekkers, M.J., Guo, Z., Waldrip, R., Li, X., Zhang, X., Liu, D., Kapp, P., 2015. Can a primary remanence be retrieved from partially remagnetized Eocence volcanics in the Nanmulin Basin (Southern Tibet) to date the India–Asia collision? J. Geophys. Res., Solid Earth 120. http://dx.doi.org/10.1002/2014JB011599.

Jackson, M.J., Banerjee, J.A., Marvin, R.L., Grueber, W., 1991. Detrital remanence inclination errors, and anhysteretic remanence anisotropy: quantitative model and experimental results. Geophys. J. Int. 104, 95–103.

Kodama, K.P., 1997. A successful rock magnetic technique for correcting paleomagnetic inclination shallowing: case study of the Nacimiento Formation, New Mexico. J. Geophys. Res., Solid Earth 102, 5193–5205. http://dx.doi.org/10.1029/5196JB03833.

Kodama, K.P., 2009. Simplification of the anisotropy-based inclination correction technique for magnetite- and haematite-bearing rocks: a case study for the Carboniferous Glenshaw and Mauch Chunk Formations, North America. Geophys. J. Int. 176, 467–477.

Kruiver, P.P., Dekkers, M.J., Heslop, D., 2001. Quantification of magnetic coercivity components by the analysis of acquisition curves of isothermal remanent magnetisation. Earth Planet. Sci. Lett. 189, 269–276.

Lee, H.Y., Chung, S.L., Lo, C.H., Ji, J., Lee, T.Y., Qian, Q., Zhang, Q., 2009. Eocene Neotethyan slab breakoff in southern Tibet inferred from the Linzizong volcanic record. Tectonophysics 477, 20–35.

Lippert, P.C., van Hinsbergen, D.J.J., Dupont-Nivet, G., 2014. The Early Cretaceous to Present latitude of the central Lhasa-plano (Tibet): a paleomagnetic synthesis with implications for Cenozoic tectonics, paleogeography and climate of Asia. In: Nie, J.S., Hoke, G.D., Horton, B.K. (Eds.), Towards an Improved Understanding of Uplift Mechanisms and the Elevation History of the Tibetan Plateau. In: Geological Society of America Special Paper, vol. 507, pp. 1–21.

Ludwig, K.R., 2008. Isoplot 3.60. Special Publication, vol. 4. Berkeley Geochronology Center, 77 p.

Ma, Y., Yang, T., Yang, Z., Zhang, S., Wu, H., Li, H., Li, H., Chen, W., Zhang, J., Ding, J., 2014. Paleomagnetism and U–Pb zircon geochronology of Lower Cretaceous lava flows from the western Lhasa terrane: new constraints on the India–Asia collision process and intracontinental deformation within. Asia J. Geophys. Res., Solid Earth 119, 7404–7424. http://dx.doi.org/10.1002/2014JB011362.

Maffione, M., Van Hinsbergen, D.J.J., Koornneef, L., Guilmette, C., Hodges, K.V., Huang, W., Kapp, P., Ding, L., submitted for publication. Forearc hyperextension dismembered the South Tibetan ophiolites. Geology.

Najman, Y., Appel, E., Boudagher-Fadel, M., Bown, P., Carter, A., Garzanti, E., Godin, L., Han, J., Liebke, U., Oliver, G., 2010. Timing of India–Asia collision: geological, biostratigraphic, and palaeomagnetic constraints. J. Geophys. Res., Solid Earth 115, B12416. http://dx.doi.org/10.1029/2010JB007673.

Orme, D.A., Carrapa, B., Kapp, P., 2014. Sedimentology, provenance and geochronology of the upper Cretaceous–lower Eocene western Xigaze forearc basin, southern Tibet. Basin Res. 1 (25). http://dx.doi.org/10.1111/bre.12080.

Patzelt, A., Li, H., Wang, J., Appel, E., 1996. Palaeomagnetism of Cretaceous to Tertiary sediments from southern Tibet: evidence for the extent of the northern margin of India prior to the collision with Eurasia. Tectonophysics 259, 259–284.

Pozzi, J.P., Westphal, M., Girardeau, J., Besse, J., Zhou, Y., Chen, X., Xing, L., 1984. Paleomagnetism of the Xigaze ophiolite and flysch (Yarlung Zangbo suture zone, southern Tibet): latitude and direction of spreading. Earth Planet. Sci. Lett. 70, 383–394.

Roberts, A.P., Cui, Y., Verosub, K.L., 1995. Wasp-waisted hysteresis loops: mineral magnetic characteristics and discrimination of components in mixed magnetic systems. J. Geophys. Res., Solid Earth 100, 17909–17924. http://dx.doi.org/10.1029/95JB00672.

Searle, M.P., Windley, B.F., Coward, M.P., Cooper, D.J.W., Rex, A.J., Rex, D., Li, T., Xiao, X., Jan, M.Q., Thakur, V.C., Kumar, S., 1987. The closing of Tethys and the tectonics of the Himalaya. Bull. Geol. Soc. Am. 98, 678–701.

Tan, X., Kodama, K.P., Chen, H., Fang, D., Sun, D., Li, Y., 2003. Paleomagnetism and magnetic anisotropy of Cretaceous red beds from the Tarim basin, northwest China: evidence for a rock magnetic cause of anomalously shallow paleomagnetic inclinations from Central Asia. J. Geophys. Res., Solid Earth 108, 2107. http://dx.doi.org/10.1029/2001JB001608.

Tauxe, L., Kent, D.V., 2004. A simplified statistical model for the geomagnetic field and the detection of shallow bias in paleomagnetic inclinations: was the ancient magnetic field dipolar. In: Timescales of the Paleomagnetic Field. In: Geophysical Monograph Series, vol. 145, pp. 101–115.

Tauxe, L., Watson, G., 1994. The fold test: an eigen analysis approach. Earth Planet. Sci. Lett. 122, 331–341.

Van der Voo, R., Spakman, W., Bijwaard, H., 1999. Tethyan subducted slabs under India. Earth Planet. Sci. Lett. 171, 7–20.

van Hinsbergen, D.J.J., Kapp, P., Dupont-Nivet, G., Lippert, P.C., Decelles, P.G., Torsvik, T.H., 2011. Restoration of Cenozoic deformation in Asia and the size of Greater India. Tectonics 30, TC5003. http://dx.doi.org/10.1029/2011TC002908.

van Hinsbergen, D.J.J., Lippert, P.C., Dupont-Nivet, G., McQuarrie, N., Doubrovine, P.V., Spakman, W., Torsvik, T.H., 2012. Greater India Basin hypothesis and a two-stage Cenozoic collision between India and Asia. Proc. Natl. Acad. Sci. USA 109, 7659–7664.

Wu, F.-Y., Ji, W.-Q., Liu, C.-Z., Chung, S.-L., 2010. Detrital zircon U–Pb and Hf isotopic data from the Xigaze fore-arc basin: constraints on Transhimalayan magmatic evolution in southern Tibet. Chem. Geol. 271, 13–25.

Yang, T., Ma, Y., Zhang, S., Bian, W., Yang, Z., Wu, H., Li, H., Chen, W., Ding, J., 2014. New insights into the India–Asia collision process from Cretaceous paleomagnetic and geochronologic results in the Lhasa terrane. Gondwana Res. http://dx.doi.org/10.1016/j.gr.2014.06.010.

Yin, A., Harrison, M.T., 2000. Geologic evolution of the Himalayan–Tibetan orogen. Annu. Rev. Earth Planet. Sci. 28, 211–280.

Yin, A., Harrison, T.M., Murphy, M., Grove, M., Nie, S., Ryerson, F., Feng, W.X., Le, C.Z., 1999. Tertiary deformation history of southeastern and southwestern Tibet during the Indo–Asian collision. Bull. Geol. Soc. Am. 111, 1644–1664.

Ziabrev, S.V., Aitchison, J.C., Abrajevitch, A.V., Davis, A.M., Luo, H., 2003. Precise radiolarian age constraints on the timing of ophiolite generation and sedimentation in the Dazhuqu terrane, Yarlung–Tsangpo suture zone, Tibet. J. Geol. Soc. 160, 591–599.